

# Geophysical Research Letters®

## RESEARCH LETTER

10.1029/2021GL095138

### Key Points:

- Release of in situ electrons at the Sun is delayed from the release of hard X-ray generating electrons in impulsive SEP events
- The release delay of in-situ electrons at the Sun shows a clear energy dependence which can be fitted by a power law of electron momentum
- The power law index from the above fitting is related to the turbulence dissipation range spectral index at the flare site

### Correspondence to:

G. Li,  
[gangli.uah@gmail.com](mailto:gangli.uah@gmail.com)








### Citation:

Li, G., Wu, X., Effenberger, F., Zhao, L., Lesage, S., Bian, N., & Wang, L. (2021). Constraints on the electron acceleration process in solar flare: A case study. *Geophysical Research Letters*, 48, e2021GL095138. <https://doi.org/10.1029/2021GL095138>

Received 13 JUL 2021

Accepted 23 SEP 2021

## Constraints on the Electron Acceleration Process in Solar Flare: A Case Study

G. Li<sup>1</sup> , X. Wu<sup>1,2</sup> , F. Effenberger<sup>3,4</sup> , L. Zhao<sup>5</sup> , S. Lesage<sup>1</sup> , N. Bian<sup>1</sup> , and L. Wang<sup>6</sup> 

<sup>1</sup>Department of Space Science and Center for Space Plasma and Aeronomic Research, University of Alabama in Huntsville, Huntsville, AL, USA, <sup>2</sup>School of Geophysics and Information Technology, China University of Geoscience, Beijing, People's Republic of China, <sup>3</sup>Institut für Theoretische Physik, IV, Ruhr-Universität Bochum, Bochum, Germany, <sup>4</sup>Previously at Helmholtz Center Potsdam, GFZ, German Research Center for Geosciences, Potsdam, Germany, <sup>5</sup>Department of Climate and Space Sciences and Engineering (CLASP), University of Michigan, Ann Arbor, MI, USA, <sup>6</sup>School of Earth and Space Sciences, Peking University, Beijing, People's Republic of China

**Abstract** Combining in situ measurements of energetic electrons and remote sensing observations of hard X-rays and type III radio bursts, we examine the release times of energetic electrons in the July 23, 2016 event. We find that the releases of in situ energetic electrons from the Sun are delayed from those electrons that are responsible for the hard X-rays. We further find that the release time of in situ electrons is a function of electron energy. Under the assumption that the acceleration mechanism for the upward propagating electrons is of Fermi-type and is controlled by an energy-dependent diffusion coefficient, we fit these release times by a simple functional form, related to the turbulence spectral index. Implications of our study on the underlying electron acceleration mechanisms and the magnetic reconnection process in solar flares are discussed. Our results demonstrate the power of the recently developed fractional velocity dispersion analysis (FVDA) method in solar flare studies.

**Plain Language Summary** Solar flares are efficient particle accelerators. Electrons and ions are accelerated to very high energies at solar flares. Magnetic reconnection is believed to be the main energy convertor at solar flares. Observations and simulations in the past decade have shown that when magnetic reconnection occurs, electrons can be accelerated at both the reconnection site and the reconnection exhausts, which are plasma shooting away from the reconnection site. Energetic electrons precipitating down on the solar surface will cause hard X-ray and gamma ray. Energetic electrons escape outward can be observed in situ. Are these two populations of electron released at the same reconnection site, or they have different acceleration history, perhaps at the two oppositely propagating exhausts? In this study, we examine this question using timing studies of in-situ electrons and hard X-ray observations of the solar flare from Fermi observation. We show that outward propagating electrons are undergoing a longer acceleration process than those downward propagating electrons, suggesting an acceleration process that is volume-filling and is consistent with a second-order Fermi acceleration at the reconnection exhaust propagating upward.

## 1. Introduction

Solar flares are a major particle accelerator in the solar system (Reames, 2015). In the standard flare model (aka CSHKP model) (Carmichael, 1964; Hirayama, 1974; Kopp & Pneuman, 1976; Sturrock, 1966), magnetic reconnection at the reconnection current sheet powers the particle acceleration process. Recent RHESSI imaging observations (Liu et al., 2013) have revealed that energetic electrons may be accelerated at reconnection exhausts. It is possible that energetic electrons propagating downward and upward undergo different acceleration processes. In the standard flare model, the reconnection is between close field lines so electrons accelerated in the upward propagating reconnection exhaust can not reach 1 AU unless interchange reconnection is involved (Masson et al., 2013) (Note that however, a closed loop from a preceding CME can extend beyond 1 AU. If magnetic reconnection occurs between the two legs of this closed loop, then electrons can propagate into 1 AU along a closed loop). Electrons can be accelerated at these interchange reconnection sites as well. In the early work of Heyvaerts et al. (1977), flares are driven by interchange reconnection alone, without closed field reconnection. One important implication of Heyvaerts et al. (1977)

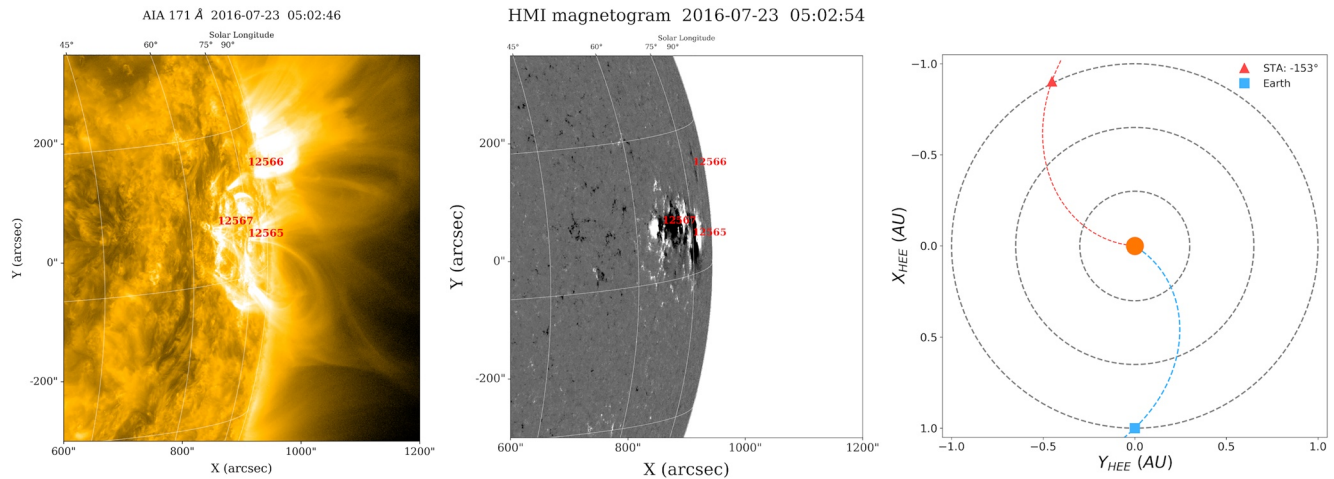


**Figure 1.** Left and middle panels: the Solar Dynamics Observatory (SDO)/Atmosphere Imaging Assembly (AIA) and SDO/Helioseismic and Magnetic Imager (HMI) images showing the AR 12565 right before the eruption. Three ARs can be seen in the figure and the AR12565 was located at N07W75. Right panel: the location of the Earth and STEREO-A in this event.

is that electrons propagating downward and upward are released from the reconnection acceleration at the same time.

Li et al. (2020) compared the release times of in-situ energetic electrons with those of hard X-ray generating electrons for the April 25, 2001 event. They found that the upward propagating electrons were delayed by  $\sim 8$  min from those precipitating down to the solar surface. Li et al. (2020) concluded that in situ electrons and hard X-ray generating electrons are two different populations.

In this Letter, we extend the analysis in Li et al. (2020) and examine the release times of the downward precipitating electrons and those upward escaping electrons for the July 23, 2016 event. Comparing to Li et al. (2020), we not only use in situ wind/3DP electron measurements, but also take into account Fermi/GBM hard X-ray measurements and type III radio bursts observations from Wind and STEREO-A to provide us better timing constraint in this study. Using Fermi/GBM observation, we obtain the release times for hard X-ray generating electrons and show that these times precede the release times of outward propagating electrons. We find the latter release times have a simple energy dependence, which can be fitted by a power-law form as given in Equation 4. The fitting parameter  $\gamma$  is related to the turbulence power spectrum index at the acceleration site. Our study therefore outlines a way to remotely examine the MHD turbulence at the acceleration site.

## 2. Observations

An M7.6 flare, from AR 12565 erupted on July 23, 2016 around 05:05:40 UT. The flare was well observed by the Atmosphere Imaging Assembly (AIA, Lemen et al., 2012) and the Helioseismic and Magnetic Imager (HMI, Schou et al., 2012) onboard the Solar Dynamics Observatory (SDO, (Pesnell et al., 2012)). Hard X-rays were also captured by Fermi/GBM, which consists of 12 Sodium Iodide (NaI) detectors covering the energies 8–1,000 keV, and two Bismuth Germanate (BGO) detectors covering the energies of 200 keV–40 MeV (Meegan et al., 2009). HXRs were also observed by the Ramaty High Energy Solar Spectroscopic Imager (RHESSI) which yields similar profiles to that of Fermi/GBM. Fermi/GBM has finer time resolution ( $<1$  s) and better signal, so we use Fermi/GBM observations in our study. Type III radio bursts from Wind/WAVE and STEREO-A/WAVE (Bougeret et al., 1995, 2008) were also observed. In situ energetic electrons was observed by the 3D Plasma and Energetic Particle (3DP) instruments onboard Wind spacecraft (Lin et al., 1995).

Left and middle panels of Figure 1 plot the SDO/AIA (171 Å) and SDO/HMI images of AR12565 before the eruption. AR12565 was located at N07W75 and is indicated in both panels in Figure 1. Another two nearby

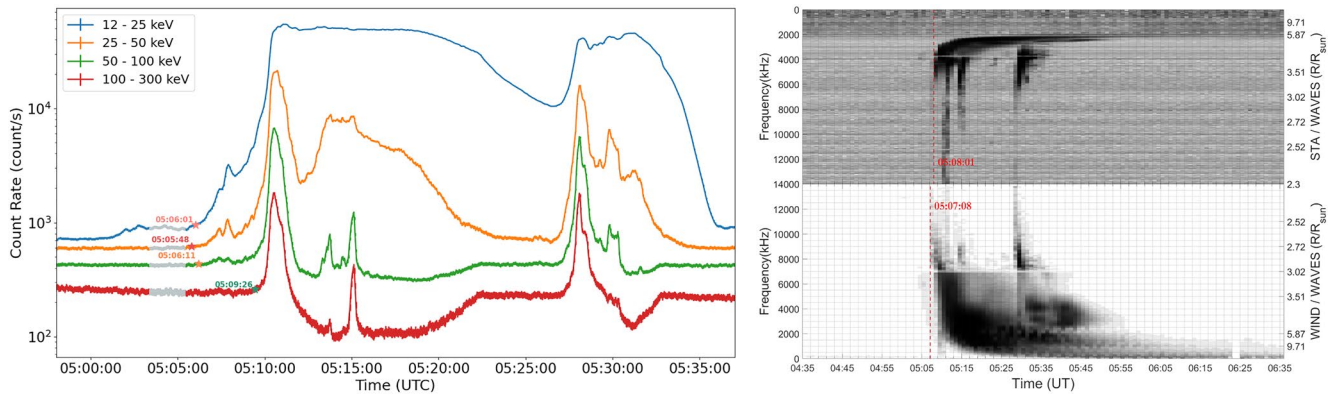


**Figure 2.** Left: Hard X-ray intensities for four energy channels from 5:00 to 5:35. The periods in silver denote the background periods from which the average and standard deviation  $\sigma$ s are calculated. Right: Type III radio bursts observed by the WAVE instruments onboard of Wind (lower panel) and STA (upper panel). The red dashed line indicates the onset of the type III radio bursts.

ARs were also labeled. This is a typical impulsive flare. In the right panel of Figure 1, the locations of the Earth and spacecraft STEREO-A are shown. STEREO-A is a  $153^\circ$  to the east of the Earth.

The left panel of Figure 2 shows the hard X-ray intensity from 5:00 to 5:35 UT measured by FERMI/GBM with a time resolution of 1 s. Data of four energy channels 10 – 25 keV, 25 – 50 keV, 50 – 100 keV, and 100 – 300 keV are shown in blue, brown, green, and red, respectively. The time periods in silver indicate the backgrounds, which is taken to be a 2-min period from 05:03:24 to 05:05:24. For each energy channel, the onset time is identified from the end of the background period forward as the time when the intensity is  $3\sigma$  above the background average. These times are used as proxies for the release times of downward-propagating electrons from the acceleration site. Saturation effect, in the form of a dip in the intensity between 05:11 and 05:23, can be spot in the high-energy channel (red curve). However, this does not affect the determination of the onset times since only data at the beginning of the event (before the peak) are used.

Hard X-rays are generated by the interaction of high-energy electrons with the sun's atmosphere. Electrons of energy  $E$  can generate hard X-rays with energy  $E' \leq E$ . Therefore, the time profiles of hard X-rays represent energy-integrated solar atmosphere response to the precipitating electrons. Consequently, we use the three-sigma threshold, not the FVDA, to obtain the onset times. From Figure 2, we see that the hard X-ray onset times for the 12 – 25, 25 – 50, and 50 – 100 keV channels are practically the same, and are  $\sim 3$  min earlier than the  $\geq 100$  keV channel. This timing sequence is consistent with a scenario where electrons up to 100 keV are accelerated at the downward propagating reconnection exhaust, and a further acceleration at a termination shock for  $\geq 100$  keV electrons (Guo et al., 2017; Li et al., 2013). Also, see Figure 5.

The distance between the Sun and the Earth was 1.016 AU during this event, which translates to a light travel time of 8 min and 27 s. Subtracting this from the observed times yields the release times of the parent electrons from the acceleration site. The right panel of Figure 2 shows the type III radio observations from Wind/WAVES and STA/WAVES, with a time resolution of 1 min. Type III radio bursts are generated at plasma frequency  $f_p$  (or its second harmonic) when fast electron beam propagates along open field lines (Wild et al., 1963). The generation depends on both the energy of electrons and the anisotropy of the beam. In Krucker et al. (2011), an energy range of 1–30 keV was assumed for type-III generating electrons. In the work of Cairns et al. (2018), a broader energy range, 2.5–125 keV, corresponding to an electron speed from 0.1 to 0.7c, was assumed as type-III generating electrons. Taking a flare temperature to be 10 (20) million degrees, that is, a thermal energy of  $\sim 3k_B T \sim 2.5$  (5.0) keV, and assuming type-III radio bursts are caused by non-thermal electron population with a speed two times faster than average thermal speed, then type-III generating electrons have an energy of  $\sim 10$  (20) keV. In this work, we assume a type-III generating electron to have an energy range of (10, 22.5) keV, corresponding to a speed range of (0.2c, 0.3c) or a momentum range of (0.10, 0.15) MeV/c. The red dashed line in the right panel of Figure 2 marks the onset time of the type-III, 05:07:08, corresponding to a release time of 04:58:39 near the Sun. Note that we implicitly assume that the electrons observed in-situ are also the type-III generating electrons. This needs not to be the case.

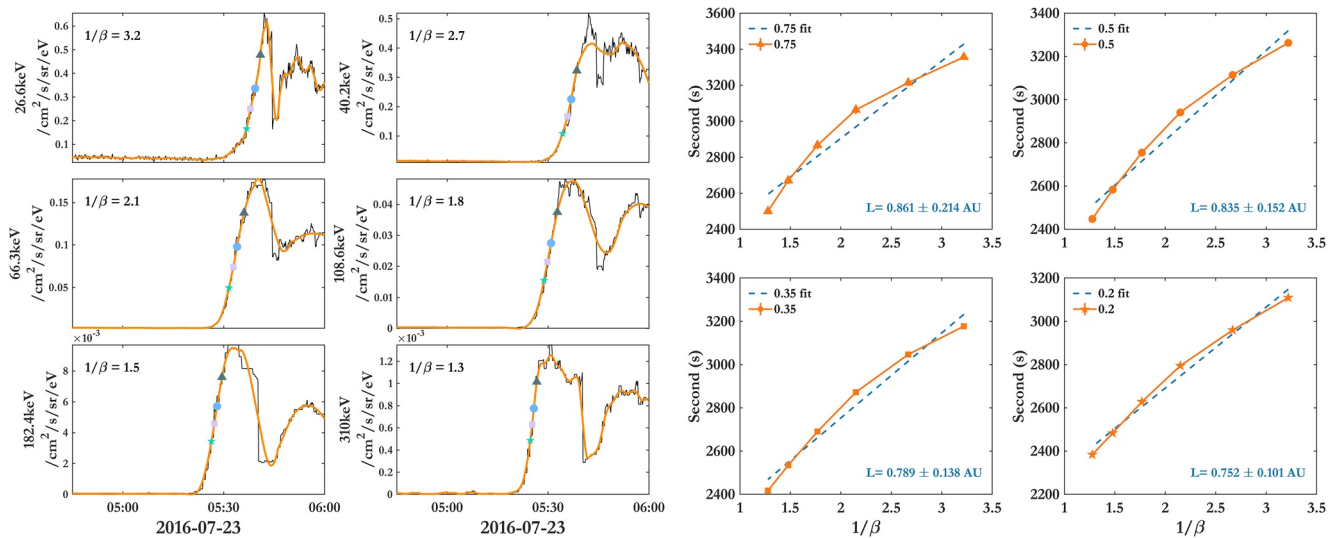


**Figure 3.** Left: energetic electrons observed by Wind/3DP. Reference points for  $\eta = 0.2, 0.35, 0.5,$  and  $0.75$  are labeled. Right: the fractional velocity dispersion analysis (FVDA) analysis for the four  $\eta$ s shown in the left panel. The fitted path length and its uncertainty are shown in each panel.

We next use the FVDA method (Li et al., 2020; Zhao et al., 2019) to examine the release times of in-situ energetic electrons. The FVDA method makes use of the entire fast-rising phase of the electron time intensity profiles instead of relying only on the hard-to-determine onset times. For all energy bins, we identify points with intensities that are a fraction  $\eta$  of the peak intensities and then we apply the VDA for these points. The  $\eta$  dependence of the path length allows one to obtain a better estimate of the path length by taking  $\eta \rightarrow 0$ . In the traditional VDA, since only one path length is determined (corresponding to a single  $\eta$ , sometimes taken at  $\eta = 1$  which corresponds to the peak intensity), one cannot tell if a smaller-than-1 AU path length is due to analysis uncertainty. Using the FVDA, however, the result is more trustworthy. Furthermore a clear trend of a decreasing  $L(\eta)$  with decreasing  $\eta$  is story-telling of an energy-dependent release (Li et al., 2020) and has been used in selecting this event.

In Figure 3, the left panel shows the rising phase of the event for six energy bins. Reference points corresponding to a fraction  $\eta$  of the peak for  $\eta = 0.75, 0.5, 0.35,$  and  $0.2$  are labeled as solid “triangle,” “circle,” “square,” and “star” in the plots. The right panel of Figure 3 shows the FVDA analysis for the four  $\eta$ s. We see that the fitted path length  $L$ 's, with uncertainty, are shorter than 1 AU for all four  $\eta$ s. As shown in Li et al. (2020); Zhao et al. (2019), a path length systematically smaller than 1 AU for multiple  $\eta$ s from FVDA is a sign indicating that the release of energetic electrons at the Sun is energy-dependent. Simulations by Moradi and Li (2019) have shown that path lengths of electrons in impulsive events can be regarded as energy independent. Therefore, for any given path length, we can obtain the release times of electrons at the Sun as a function of energy (Li et al., 2020). Assuming the onset time of type III radio bursts to be a proxy of that of 15 keV electrons, we obtain a range of path length from 1.0 to 1.35 AU, with 1.15 AU the nominal Parker path length using the 2-h average solar wind speed prior to the in situ electrons.

In the left panel of Figure 4, the deduced release times of in-situ energetic electrons at the Sun are shown as red circles, blue squares, and green diamonds for three choices of path length: 1.25, 1.15, and 1 AU, respectively. The energies of these electrons are 27, 40, 66, 109, 182, and 300 keV. The release time uncertainties from the fitting are smaller than the symbol size. For the case of  $L = 1.15$  AU, these uncertainties are 5, 13, 11, 6, 8, 7 s, energy from low to high, respectively. The stars in the left are the onset times from the hard X-ray observations in Figure 2. Uncertainties of these times are also small. The pink star indicates the onset time of the type III radio bursts and the uncertainty is 1 min. Clearly, the release times of the upward propagating electrons are delayed from those downward propagating electrons. Moreover, the release times of upward propagating electrons show a clear energy dependence with electrons of higher energy released at later times.



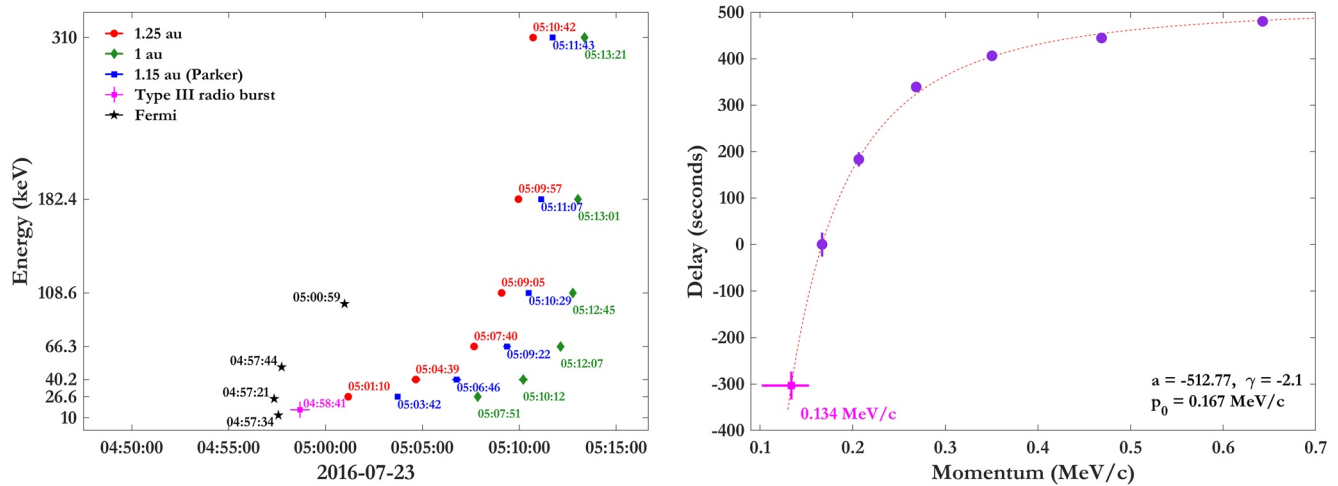


**Figure 4.** Left: The release times of energetic electrons for different energies. The time of downward, Hard X-ray generating electrons are labeled as black stars. The type III time is labeled as the pink star. The red circles, blue squares, and green diamonds are release times of energetic electrons observed in-situ, assuming a path length of 1.25, 1.15, and 1.0 AU, respectively. Right: The delay of onset times as defined in Equation 1 with  $p_0 = 0.167$  MeV/c, corresponding to  $T = 27$  keV, assuming a path of 1.15 AU. The energies of type-III generating electrons are assumed to be in the range of 10–22.5 keV (a momentum of 0.10–0.15 MeV/c).

Using the release time of  $p_0 = 0.167$  MeV/c (corresponding to  $E_0 = 27$  keV) electrons as a reference, we compute the delay time as a function of electron momentum,

$$\Delta t(p; p_0) = t_{rel}(p) - t_{rel}(p_0) \quad (1)$$

We consider the case with a path length of  $L = 1.15$  AU. Results are similar for other cases. The right panel of Figure 4 shows  $\Delta t(p; p_0)$ . The momentum dependence of the release time delay is due to both acceleration and escape/trapping, and can be written as,

$$\Delta t(p; p_0) = (t_{acc}(p) - t_{acc}(p_0)) + (t_{esc}(p) - t_{esc}(p_0)). \quad (2)$$

In the right hand side, the first term is due to acceleration, the second term due to escape/trapping. Petrosian (2012); Effenberger and Petrosian (2018) have considered the interplay of acceleration and trapping. In solar flares, the acceleration can be of either the first-order Fermi (i.e., shock acceleration) or the second-order Fermi (acceleration by turbulence at flare site). In both cases, the spatial diffusion coefficient  $\kappa(p)$  is a crucial parameter that determines the acceleration and escape/trapping. In the case of first-order Fermi acceleration, the acceleration time scale can be estimated through,

$$dt_{acc} \sim (\kappa/U^2) * dp/p, \quad (3)$$

where  $U$  is the upstream flow speed in the shock frame (Drury, 1983). In the case of second-order Fermi acceleration, the shock speed  $U$  in Equation 3 needs to be replaced by the Alfvén speed  $V_A$  (Petrosian, 2012). For the escape/trapping time scale, one can estimate it from the following consideration: assuming the accelerated electrons are confined spatially, and has to go through a diffusion (i.e., random walk) process to access earth-connecting open field lines that are at a distance  $l$  from the acceleration site, then the time associated with the trapping is  $\delta t_{esc} \sim (l/\lambda)^2 (\lambda/v) = l^2/\kappa(p)$  with  $v$  electron speed and  $\lambda$  mean free path. Note that  $\delta t_{acc}$  is proportional to  $\kappa$  and  $\delta t_{esc}$  is inversely proportional to  $\kappa$ . Assuming  $\kappa \sim p^\gamma$ , one can integrate Equation 3 to obtain the following functional form of  $\Delta t$ ,

$$\Delta t(p; p_0) = \text{sign}(\gamma) a \left[ \left( \frac{p}{p_0} \right)^\gamma - 1 \right] + b \left[ \left( \frac{p}{p_0} \right)^{-\gamma} - 1 \right] \quad (4)$$

In flare sites, energetic electrons interact with broad-band turbulence whose spectrum can be approximated as  $k^{-\epsilon}$ . Under the framework of quasi-linear theory QLT (Jokipii, 1966), one finds  $\gamma = 3 - \epsilon$ . The spectral index  $\epsilon$  in the inertial range varies slightly from  $\sim 1.5$  (Kraichnan-like) to  $\sim 1.7$  (Kolmogorov-like). It is steeper and varies significantly in the dissipation range. Electrons interact mostly with turbulence in the dissipation range. Dröge (2003) examined multiple electron events and found that  $\epsilon$  in the dissipation range can be as large as 4.5. Such a large  $\epsilon$  has also been reported by Alexandrova et al. (2009); Sahraoui et al. (2010). Recent studies by Mallet et al. (2017); Vech et al. (2018) suggested that magnetic reconnection can lead to a steeper spectral index at scale just above the dissipation scale. Using Equation 4, one can fit the time delay to obtain  $\gamma$  and therefore  $\epsilon$ , providing an indirect way of probing the nature of the turbulence at the flare site. We note that in Equation 4, the acceleration may dominate the escape/trapping or vice versa. For our event, fitting the time delay yields,

$$\Delta t(p) = 512 \left[ 1 - \left( \frac{p_0}{p} \right)^{2.10} \right] \text{ sec}, \quad p_0 = 0.167 \text{ MeV}/c, \quad (5)$$

where the delay due to trapping is negligible. The fitted curve is shown as the red dashed line in the right panel of Figure 4. Equation 4 contains only two free parameters,  $a$  and  $\gamma$  ( $p_0$  is chosen) where  $a$  is an overall amplitude, and  $\gamma$  decides the shape. All six data points are fitted nicely by Equation 5. The release time of the type-III generating electrons also lies on this curve, shown as the pink star. The fitting result of  $\gamma = -2.1$  implies that  $\epsilon = 5.1$ . This value is somewhat larger than 4.5 in that reported, for example, by Sahraoui et al. (2010). However, as noted by Vech et al. (2018), a steeper spectrum is expected when reconnection occurs. They argue that below a disruption scale, reconnection leads to vortex-like structures, which accelerates the cascading, and to maintain a constant energy cascading rate a steeper spectrum must develop. Since flare is driven by magnetic reconnection, our finding of a  $\epsilon$  close to five is not surprising. Note that a spectrum steeper than  $k^{-3}$  implies that the acceleration process becomes faster when electron energy increases. This, of course, cannot continue indefinitely because when an electron's energy exceeds a threshold, the electron will resonate with the inertial range of the turbulence. Such a behavior was noted by Li et al. (2013) as a possible explanation of the spectral hardening above  $\sim 500$  keV of hard X-rays in solar flares.

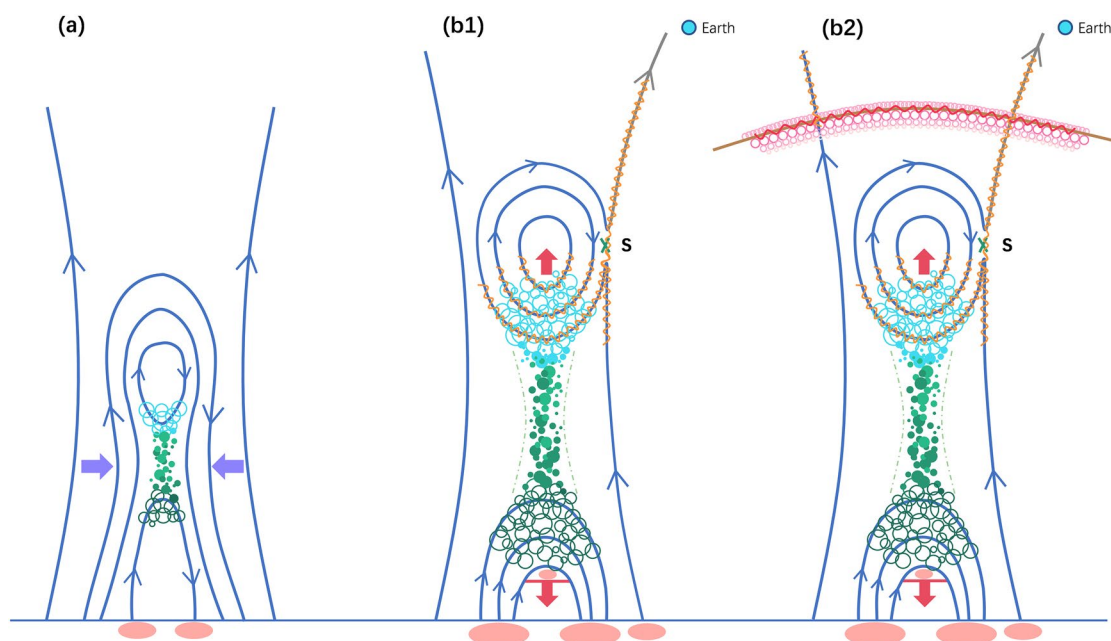


**Figure 5.** 2D cartoon showing the underlying acceleration of energetic electrons in solar flares. See text for details.

### 3. Discussion and Conclusions

In this letter, we examine the release times of energetic electrons in the July 23, 2016 impulsive SEP event using Hard X-ray data from Fermi/GBM, type III radio bursts from Wind and STA, and in situ electron data from Wind. Employing the recently developed FVDA, we find that the release of upward propagating electrons are delayed from those precipitating down to the solar surface. Furthermore, the release times for these electrons are energy dependent, and can be fitted by a simple functional form as shown in Equation 4 with a parameter  $\gamma = -2.1$ , which we relate to a  $\sim k^{-5.1}$  dissipation range of the MHD turbulence power spectrum at the acceleration site.

These results can be used to put constraints on the underlying electron acceleration process at solar flares. First, we note that the delay between the upward and downward propagating electrons likely indicates that these two electrons are of different populations, that is, they are accelerated at different sites. This confirms our previous finding from the April 25, 2001 event (Li et al., 2020). In studying the July 19, 2012 event, Liu et al. (2013) noticed that bidirectional outflows were associated with spatially separated coronal X-ray sources, and proposed that electrons are accelerated mainly in the upward and downward propagating reconnection exhausts than in the reconnection region itself. Our timing study is consistent with the finding of Liu et al. (2013). Because the plasma environments in the downward and upward exhausts are different, one expects that the acceleration time scales at these two exhausts differ.

From our analysis in Equations 4 and 5, the time delay due to trapping is negligible, implying that the interchange reconnection must occur close in time to the main reconnection. Our study suggests a solar flare scenario as illustrated in Figure 5. In this scenario, a solar flare is triggered by a magnetic reconnection between closed loops. This is the main reconnection, which is associated with plasma heating. Efficient electron acceleration occurs in the two oppositely propagating reconnection exhausts. Electrons accelerated in the downward propagating exhaust precipitate to the solar surface and cause hard X-rays, as shown in panel (a) of Figure 5. As the reconnection continues, shown in panel (b1) of Figure 5, the separation between the footpoints of the post flare loops increase; the upward propagating reconnection exhaust expands, triggering an interchange reconnection; electrons accelerated in the upward propagating exhaust can access open field lines through this interchange reconnection, and be observed in situ. Propagating downward, they could lead to a third hard X-ray footpoint (see e.g., Krucker & Lin, 2002; Vilmer et al., 2002). Note that although the upward and downward reconnection exhausts are different acceleration sites, the acceleration mechanism at both sites are the same, and the accelerated electron spectra in both sites can be similar. Wang et al. (2021) examined 16 impulsive electron events observed by Wind/3DP and found that there is positive correlation between the HXR-producing electron spectral index and that of the high-energy in-situ electrons. Upward moving plasmoid can drive a coronal shock and add a further acceleration site to our scenario. This is illustrated in panel (b2) of Figure 5.

Our proposed scenario is consistent with recent radio observations of the September 10, 2017 flare (Chen et al., 2020; Gary et al., 2018). Observations of the September 10, 2017 event using the newly completed Expanded Owens Valley Solar Array microwave (MW) imaging spectroscopy by Gary et al. (2018) and Chen et al. (2020) have shown that there were low frequency MW source (see Figure 2b of Gary et al., 2018) that was higher up from the hard X-ray source, which may signal the upward propagating reconnection exhaust.

In a previous event study (Li et al., 2020), we found that the release time of in-situ energetic electrons are delayed from those precipitating downward to the solar surface. In our current study, a similar delay is found. This may suggest that such a delay could be a ubiquitous phenomenon in solar flares. Besides confirming this delay, a new result from our current study is the parameter  $\gamma$  in Equation 4, which, under the assumption of a Fermi-type acceleration and an energy-dependent diffusion coefficient  $\kappa(p)$ , is related to the turbulence spectral index  $\epsilon$  of  $k^{-\epsilon}$  in the dissipation range at the acceleration site. Within the framework of QLT,  $\epsilon = 3 - \gamma$ . Our study, therefore, outlines a procedure to probe the MHD turbulence spectrum in flare sites.

### Data Availability Statement

The in situ energetic electron data used in this work can be freely downloaded from the NASA space physics data facility at <https://cdaweb.gsfc.nasa.gov/index.html/> by selecting the Wind spacecraft and then specifying the 3DP instrument. The hard X-ray data can be downloaded from the Fermi/GBM online data repository at <http://heasarc.gsfc.nasa.gov/FTP/fermi/data/gbm/>.

## Acknowledgments

This work is supported in part by NASA grants 80NSSC19K0075, and 80NSSC19K0079 at UAH; 80NSSC19K0076, 80NSSC18K0644, 80NSSC20K0286, and 80NSSC20K0298 at UM. L. Wang is supported in part by NSFC under contracts 41774183, 41861134033. F. Effenberger acknowledges support from NASA grant NNX17AK25G and DFG grant EF 98/4-1.

## References

- Alexandrova, O., Saur, J., Lacombe, C., Mangeney, A., Mitchell, J., Schwartz, S. J., & Robert, P. (2009). Universality of solar-wind turbulent spectrum from MHD to electron scales. *Physical Review Letters*, *103*(16), 165003. <https://doi.org/10.1103/PhysRevLett.103.165003>
- Bougeret, J. L., Goetz, K., Kaiser, M. L., Bale, S. D., Kellogg, P. J., Maksimovic, M., et al. (2008). S/WAVES: The radio and plasma wave investigation on the STEREO mission. *Space Science Reviews*, *136*(1–4), 487–528. <https://doi.org/10.1007/s11214-007-9298-8>
- Bougeret, J. L., Kaiser, M. L., Kellogg, P. J., Manning, R., Goetz, K., Monson, S. J., et al. (1995). Waves: The radio and plasma wave investigation on the wind spacecraft. *Space Science Reviews*, *71*(1–4), 231–263. <https://doi.org/10.1007/BF00751331>
- Cairns, I. H., Lobzin, V. V., Donea, A., Tingay, S. J., McCauley, P. I., Oberoi, D., et al. (2018). Low altitude solar magnetic reconnection, type III solar radio bursts, and X-ray emissions. *Scientific Reports*, *8*, 1676. <https://doi.org/10.1038/s41598-018-19195-3>
- Carmichael, H. (1964). *Physics of solar flares* (p. 451).
- Chen, B., Shen, C., Gary, D. E., Reeves, K. K., Fleishman, G. D., Yu, S., et al. (2020). Measurement of magnetic field and relativistic electrons along a solar flare current sheet. *Nature Astronomy*, *4*, 1140–1147. <https://doi.org/10.1038/s41550-020-1147-7>
- Dröge, W. (2003). Solar particle transport in a dynamical quasi-linear theory. *The Astrophysical Journal*, *589*(2), 1027–1039. <https://doi.org/10.1086/374812>
- Drury, L. O. (1983). REVIEW ARTICLE: An introduction to the theory of diffusive shock acceleration of energetic particles in tenuous plasmas. *Reports on Progress in Physics*, *46*(8), 973–1027. <https://doi.org/10.1088/0034-4885/46/8/002>
- Effenberger, F., & Petrosian, V. (2018). The relation between escape and scattering times of energetic particles in a turbulent magnetized plasma: Application to solar flares. *The Astrophysical Journal*, *868*(2), L28. <https://doi.org/10.3847/2041-8213/aadb3>
- Gary, D. E., Chen, B., Dennis, B. R., Fleishman, G. D., Hurford, G. J., Krucker, S., et al. (2018). Microwave and hard X-ray observations of the 2017 September 10 solar limb flare. *The Astrophysical Journal*, *863*(1), 83. <https://doi.org/10.3847/1538-4357/aad0ef>
- Guo, L., Li, G., Reeves, K., & Raymond, J. (2017). Solar flare termination shock and synthetic emission line profiles of the Fe XXI 1354.08 Å Line. *The Astrophysical Journal*, *846*(1), L12. <https://doi.org/10.3847/2041-8213/aa866a>
- Heyvaerts, J., Priest, E. R., & Rust, D. M. (1977). An emerging flux model for the solar phenomenon. *The Astrophysical Journal*, *216*, 123–137. <https://doi.org/10.1086/155453>
- Hirayama, T. (1974). Theoretical model of flares and prominences. I: Evaporating flare model. *Solar Physics*, *34*(2), 323–338. <https://doi.org/10.1007/BF00153671>
- Jokipii, J. R. (1966). Cosmic-ray propagation. I. Charged particles in a random magnetic field. *The Astrophysical Journal*, *146*, 480. <https://doi.org/10.1086/148912>
- Kopp, R. A., & Pneuman, G. W. (1976). Magnetic reconnection in the corona and the loop prominence phenomenon. *Solar Physics*, *50*(1), 85–98. <https://doi.org/10.1007/BF00206193>
- Krucker, S., Kontar, E. P., Christe, S., Glesener, L., & Lin, R. P. (2011). Electron acceleration associated with solar jets. *The Astrophysical Journal*, *742*(2), 82. <https://doi.org/10.1088/0004-637X/742/2/82>
- Krucker, S., & Lin, R. P. (2002). Relative timing and spectra of solar flare hard X-ray sources. *Solar Physics*, *210*(1), 229–243. <https://doi.org/10.1023/A:1022469902940>
- Lemen, J. R., Title, A. M., Akin, D. J., Boerner, P. F., Chou, C., Drake, J. F., et al. (2012). The atmospheric imaging assembly (AIA) on the solar dynamics observatory (SDO). *Solar Physics*, *275*(1–2), 17–40. <https://doi.org/10.1007/s11207-011-9776-8>
- Li, G., Kong, X., Zank, G., & Chen, Y. (2013). On the spectral hardening at GSIM 300 keV in solar flares. *The Astrophysical Journal*, *769*(1), 22. <https://doi.org/10.1088/0004-637X/769/1/22>
- Li, G., Zhao, L., Wang, L., Liu, W., & Wu, X. (2020). Identification of two distinct electron populations in an impulsive solar energetic electron event. *The Astrophysical Journal*, *900*(2), L16. <https://doi.org/10.3847/2041-8213/abb098>
- Lin, R. P., Anderson, K. A., Ashford, S., Carlson, C., Curtis, D., Ergun, R., et al. (1995). A three-dimensional plasma and energetic particle investigation for the wind spacecraft. *Space Science Reviews*, *71*(1–4), 125–153. <https://doi.org/10.1007/BF00751328>
- Liu, W., Chen, Q., & Petrosian, V. (2013). Plasmoid ejections and loop contractions in an eruptive M7.7 solar flare: Evidence of particle acceleration and heating in magnetic reconnection outflows. *The Astrophysical Journal*, *767*(2), 168. <https://doi.org/10.1088/0004-637X/767/2/168>
- Mallet, A., Schekochihin, A. A., & Chandran, B. D. G. (2017). Disruption of Alfvénic turbulence by magnetic reconnection in a collisionless plasma. *Journal of Plasma Physics*, *83*(6), 905830609. <https://doi.org/10.1017/S0022377817000812>
- Masson, S., Antiochos, S. K., & DeVore, C. R. (2013). A model for the escape of solar-flare-accelerated particles. *The Astrophysical Journal*, *771*(2), 82. <https://doi.org/10.1088/0004-637X/771/2/82>
- Meegan, C., Lichti, G., Bhat, P. N., Bissaldi, E., Briggs, M. S., Connaughton, V., et al. (2009). The Fermi gamma-ray burst monitor. *The Astrophysical Journal*, *702*(1), 791–804. <https://doi.org/10.1088/0004-637X/702/1/791>
- Moradi, A., & Li, G. (2019). Propagation of scatter-free solar energetic electrons in a meandering interplanetary magnetic field. *The Astrophysical Journal*, *887*(1), 102. <https://doi.org/10.3847/1538-4357/ab4f68>
- Pesnell, W. D., Thompson, B. J., & Chamberlain, P. C. (2012). The solar dynamics observatory (SDO). *Solar Physics*, *275*(1–2), 3–15. <https://doi.org/10.1007/s11207-011-9841-3>
- Petrosian, V. (2012). Stochastic acceleration by turbulence. *Space Science Reviews*, *173*(1–4), 535–556. <https://doi.org/10.1007/s11214-012-9900-6>
- Reames, D. V. (2015). What are the sources of solar energetic particles? Element abundances and source plasma temperatures. *Space Science Reviews*, *194*(1–4), 303–327. <https://doi.org/10.1007/s11214-015-0210-7>
- Sahraoui, F., Goldstein, M. L., Belmont, G., Canu, P., & Rezeau, L. (2010). Three dimensional anisotropic K spectra of turbulence at subproton scales in the solar wind. *Physical Review Letters*, *105*(13), 131101. <https://doi.org/10.1103/PhysRevLett.105.131101>
- Schou, J., Scherrer, P. H., Bush, R. I., Wachter, R., Couvidat, S., Rabello-Soares, M. C., & Tomczyk, S. (2012). Design and ground calibration of the helioseismic and magnetic imager (HMI) instrument on the solar dynamics observatory (SDO). *Solar Physics*, *275*(1–2), 229–259. <https://doi.org/10.1007/s11207-011-9842-2>
- Sturrock, P. A. (1966). Model of the high-energy phase of solar flares. *Nature*, *211*(5050), 695–697. <https://doi.org/10.1038/211695a0>
- Vech, D., Mallet, A., Klein, K. G., & Kasper, J. C. (2018). Magnetic reconnection may control the ion-scale spectral break of solar wind turbulence. *The Astrophysical Journal Letters*, *855*(2), L27. <https://doi.org/10.3847/2041-8213/aab351>
- Vilmer, N., Krucker, S., & Lin, R. P., & RHESSI Team. (2002). Hard X-ray and metric/decimetric radio observations of the 20 February 2002 solar flare. *Solar Physics*, *210*(1), 261–272. <https://doi.org/10.1023/A:1022492414597>
- Wang, W., Wang, L., Krucker, S., Mason, G. M., Su, Y., & Bučík, R. (2021). Solar energetic electron events associated with hard X-ray flares. *The Astrophysical Journal*, *913*(2), 89. <https://doi.org/10.3847/1538-4357/abefce>



- Wild, J. P., Smerd, S. F., & Weiss, A. A. (1963). Solar bursts. *Annual Review of Astronomy and Astrophysics*, *1*, 291. <https://doi.org/10.1146/annurev.aa.01.090163.001451>
- Zhao, L., Li, G., Zhang, M., Wang, L., Moradi, A., & Effenberger, F. (2019). Statistical analysis of interplanetary magnetic field path lengths from solar energetic electron events observed by WIND. *The Astrophysical Journal*, *878*(2), 107. <https://doi.org/10.3847/1538-4357/ab2041>